

Assessment of ATR-FTIR spectroscopy with multivariate analysis to investigate the binding mechanisms of Ag and TiO₂ nanoparticles to Chelex[®]-100 or Metsorb[™] for DGT technique

Hamid Pouran^{1*}, Rosario Perez Colodrero¹, Shuang Wu², Gary Hix¹, Julia Zakharova¹, Hao Zhang²

¹*Faculty of Science and Engineering, University of Wolverhampton. WV1 1LY, UK*

²*Lancaster Environment Centre, Lancaster University, Bailrigg, Lancaster, LA1 4YQ, UK*

***Corresponding authors:** tel.: +44 7930342062; email: hamidpouran@gmail.com

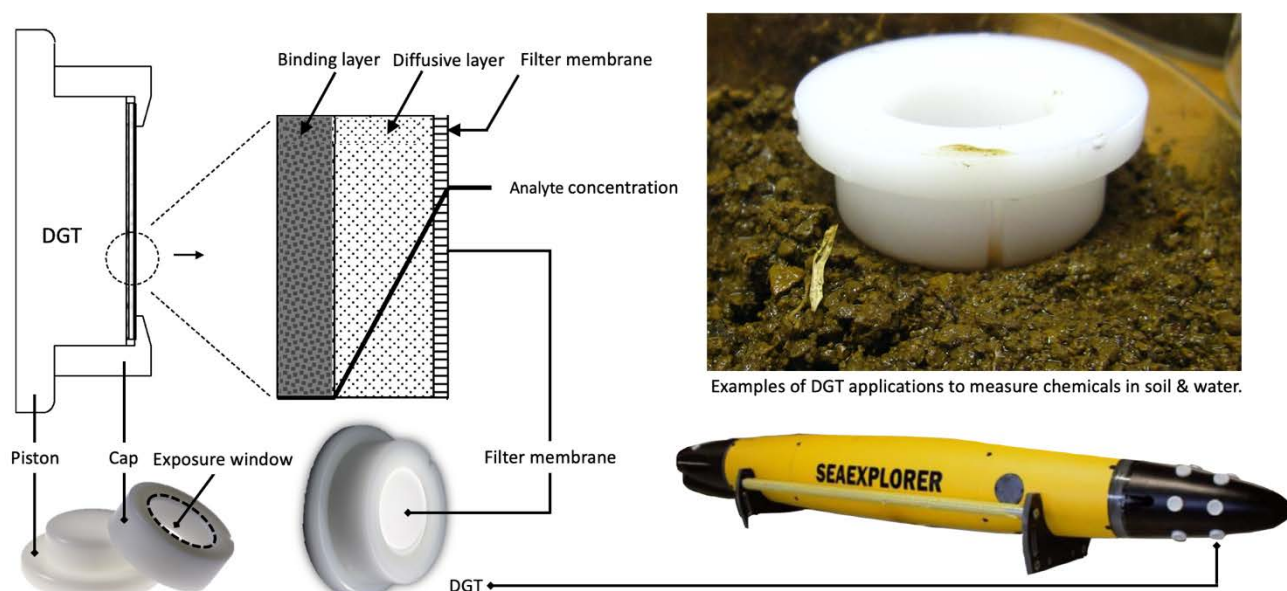
Abstract

Studying nanomaterials' ecotoxicology is not new but there are still gaps in our understanding of their fate in the environment. A major challenge is lack of reliable tools to measure available concentrations of nanoparticles (NPs) in soil and water. Diffusive gradient in thin-films (DGT) is a robust technique for measuring concentration of trace metals in the environment. We have also shown that it could be potentially developed for measuring ZnO NPs^{1,2}. To further investigate the suitability of DGT for measuring available concentrations of NPs in soil and water we selected two model nanoparticles, Ag and TiO₂ which are widely used and incorporated in different commercial products. We aimed to understand (1) if two of the DGT binding agents, Chelex®-100 and Metsorb™, could irreversibly retain our model NPs and if yes (2) what might be the differences between bound Ag and TiO₂ NPs and Ag⁺ and Ti⁴⁺ cations. We used ATR-FTIR spectroscopy for this purpose and analysed the IR spectra using principal component analysis and linear discriminant analysis (PCA-LDA), as our pattern recognition tool. The results show that the DGT resins form chemical bonds with silver and titanium nanoparticles and their ionic forms. PCA-LDA demonstrates that the binding mechanisms are statistically different (95% confidence level) among the treatments. The study indicates DGT potential for measuring available concentrations of NPs in the environment and suggests that ATR-FTIR spectroscopy combined with computational analysis could potentially differentiate between chemical species that are retained simultaneously by the DGT device resin layer.

Keywords: Attenuated total reflection-Fourier transform infrared (ATR-FTIR) spectroscopy; Diffusive gradient in thin-films (DGT); Linear discriminant analysis (LDA); Principal component analysis (PCA); Ag NP; TiO₂ NP

1. Introduction

Diffusive gradient in thin-films which is often known as DGT technique is a simple, yet accurate and reliable approach in measuring time-averaged concentrations of different chemicals in soil and water³⁻⁶. A DGT device is comprised of two key components; a diffusive hydrogel layer and a binding layer, which are protected by an external filter membrane and placed on a plastic base. A plastic cap keeps the filter membrane, the diffusive (hydrogel) and binding layer in place on top of the plastic base (piston) as illustrated in Figure 1. The function of each part of the DGT device and detailed features of them have been described extensively in previous studies^{7,8}.



The DGT technique is based on the concept that the target chemical species pass through the diffusive layer, they are irreversibly retained by the binding resin. With the

Figure 1. Schematic representation of a DGT device and its components in addition to its application in soil and water as illustrated in other research.⁶

known thicknesses of the diffusion layer, diffusion coefficients of the retained species, the surface area of the exposure window, the length of time and ambient temperature during the DGT deployment, the time averaged concentration of retained chemicals can be determined using the DGT equation, which is based on the Fick's law of diffusion.⁸

A crucial step for measuring the time-averaged concentration of a chemical by DGT is its ability to pass through the diffusive layer and being retained by the binding layer. In our previous research we showed that the DGT technique can potentially measure concentrations of manufactured nanomaterials in the environment², an approach which was promisingly repeated in other research using the same principles.⁹⁻¹³ We used combinations of different membranes and diffusive gels to allow certain sizes of particulate matters to enter the device for measuring different targeted chemical species.³ The most commonly used diffusive gels in the DGT technique are agarose, open pore polyacrylamide and restricted polyacrylamide gels. Each of them has different pore sizes. Some studies suggest that particles as large as 100 nm can diffuse through open pore hydrogel.¹⁴ For the binding layers, Chelex[®]-100, Metsorb[™] and Fe-Oxide gels are often used in the DGT devices.^{1,2,8}

We have previously studied the binding mechanism of ZnO nanoparticles (NPs) and Zn²⁺ to Chelex[®]-100 and Metsorb[™] as two commercially available and widely used binding resins.^{1,2,5} In this study, we focus on using the same resins for two industrially important and extensively made nanomaterials^{16,17}; Ag and TiO₂ nanoparticles and their ionic forms Ag⁺ and Ti⁴⁺. Chelex[®]-100 is an ion-exchange resin with efficient binding surfaces, which stems from its chemical structure. It includes dicarboxylic acid amine (COOHCH₂-NH-COOHCH₂) with carboxyl groups, which deprotonate in relatively low pH values (pH≈4).¹⁸

Less information is available about Metsorb[™] chemical structure compared to Chelex[®]. This commercial material is mainly a titanium oxide-based resin with TiO₂ and

Ti(OH)₄ as its main constituents and small quantities of other chemicals including polymers¹⁹. Both titanium oxide/hydroxide constituents in MetsorbTM have a low point of zero charge (PZC, the pH that overall surface charge is neutral); which make its surface to pose overall negative surface charge at the pH of natural environments. These pH values (PZC) are approximately 4.5 for Ti(OH)₄ and 6.0 for TiO₂.^{5,20,21}

Both Chelex[®]-100 and MetsorbTM have been used extensively as binding materials in the DGT devices for measuring targeted chemical species in soil and water⁶. We have also shown that these two resins are capable of retaining ZnO nanoparticles and potentially could be deployed for measuring nanomaterials in the environment.^{8,22} The performance of Chelex[®]-100 and MetsorbTM and their reliable function as binding materials in the DGT devices for ionic metals and nutrients have been studied before, nevertheless limited information is available about potential for nanomaterials.^{23,24} Studying the binding mechanisms of chemicals to the aforementioned resins help us to better investigate their suitability for using in the DGT technique to measure time averaged concentrations of the nanomaterials in the environment.

The aim of this research is to investigate how Chelex[®]-100 and MetsorbTM retain four different chemicals, Ag and TiO₂ nanoparticles and their ionic forms Ag⁺ and Ti⁴⁺. For this purpose, we used attenuated total reflection-Fourier transform infrared (ATR-FTIR) spectroscopy, followed by principal component analysis (PCA) and linear discriminating analysis (LDA) to further process ATR-FTIR data. ATR-FTIR spectroscopy is widely used for exploring chemical interactions at solid-liquid interfaces for both organic and inorganic samples and as a non-destructive technique.²⁵⁻²⁷ It will provide information to elucidate the underlying differences between these nanoparticles and their ionic forms chemical bonds to the DGT resins. Ag and Ti nano-particles are widely used in different industries as engineered nanomaterials. Previous studies indicate that after the waste treatment processes,

they likely re-enter the environment and accumulate in soils as their primary sink. This may lead to bioaccumulation in microorganisms and plants and affect the food chain.^{5,28} Measuring these nanomaterials concentrations in soil and water helps us to better understand their behavior in the environment.

Silver nanoparticles are well-known for their antimicrobial properties and used in many industries particularly in personal care products and clothing e.g. in textile to eliminate bacteria and odor. These nanoparticles also have unique physicochemical characteristics (e.g. electrical and thermal conductivity), which makes them attractive for many industries, for example food packaging, cosmetics and biomedical related products, that increase their risk of being released to the environment.^{29,30} Titanium dioxide nanoparticles are stable in the environment with desirable photocatalytic properties, they have high refractive index, which make them excellent white powder pigments, with extensive applications as coating or paint materials. Both of these nanomaterials have shown to have adverse environmental impacts when they are released to the environment, especially in high concentrations, which makes probing their concentrations in the environment essential.¹⁷

Experimental section

1. Material and Methods

2.1 Chemicals

TiO₂ was obtained from EVONIK (AEROXIDE® TiO₂)³¹, and Ag nanoparticles were sourced from Institut Català de Nanotecnologia, Spain. The silver nanoparticles were polyvinylpyrrolidone (PVP 9.73%) with primary particle size expected to be approximately 25nm. Detailed properties of these Ag nanoparticles, provided by the above-mentioned supplier, have been described in other studies.¹⁶ The primary particle size of the TiO₂ NPs

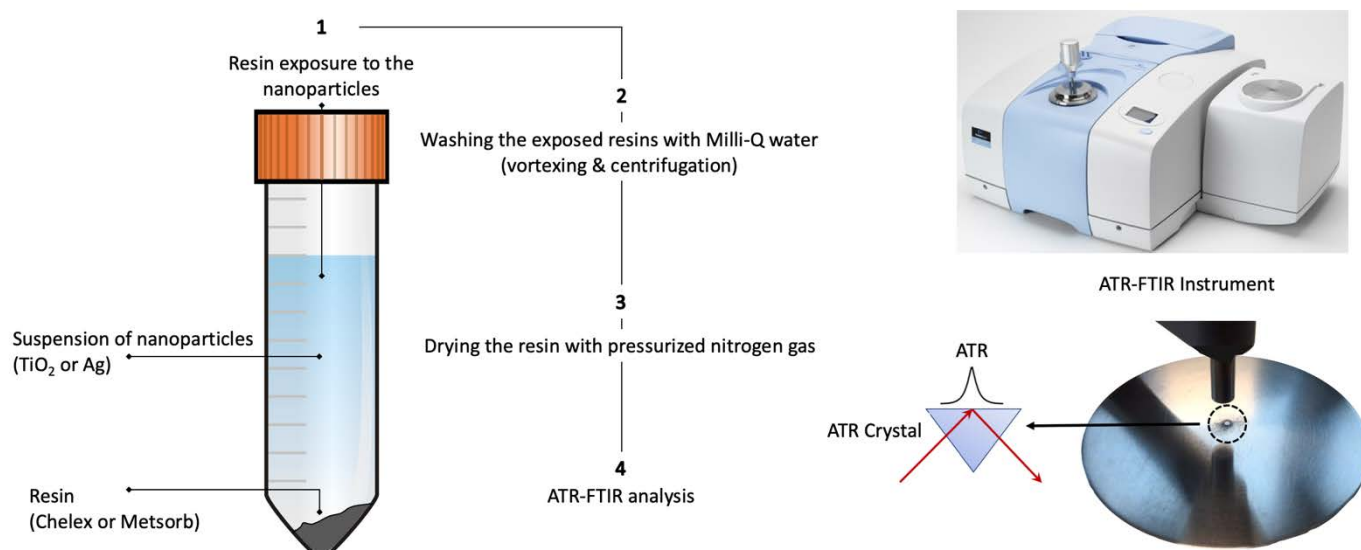
was expected to be approximately 50nm. Point of zero charge (PZC) of Ag is usually below pH \approx 4, while it is about pH \approx 6 for TiO₂ NPs,^{17,32} which create respectively negative and positive Zeta potential (electrokinetic potential) at the surface of these nanoparticles in this study. Some details can be found in supplementary information (SI). The DGT resin materials, Chelex[®]-100 and Metsorb[™] were purchased from Bio-Rad and Graver Technologies. Before each test, fresh stocks of Ag and TiO₂ nanoparticles dispersions in Milli-Q water were prepared, followed by sonication for at least 15 minutes. Fresh stocks of Ag⁺ was prepared by dissolving Sigma-Aldrich reagent grade Ag(NO₃) in Milli-Q water. For Ti⁴⁺ stock solution, acidified Sigma-Aldrich reagent grade TiCl₄ was used.

2.2 Sample preparations

Each experimental treatment for ATR-FTIR spectrochemical analysis was prepared in triplicate. For this purpose, 0.5 g of Chelex[®]-100 or Metsorb[™] (binding materials) was exposed to 20.0 ml of 1000.0 μ g/l of one of six different treatments; (1) Ag NPs, (2) Ag⁺, (3) mixture of Ag NPs and Ag⁺ (500 μ g/l each), (4) TiO₂ NPs, (5) Ti⁴⁺, (6) mixture of TiO₂ NPs and Ti⁴⁺ (500 μ g/l each), which corresponds to six different spectral classes for each of the resins. We used high concentrations for each of these treatments to enable reliable detection by ATR-FTIR spectroscopy. The pH for all the experiments in this study was approximately 5.8. For Ti⁴⁺ stock solution, which had been prepared from acidified TiCl₄, the pH was adjusted by adding very diluted NaOH solution (reagent grade). The pH were monitored for 48 hours throughout the experiments.

Each sample of a fresh chemical solution with the resin was shaken for over 3 hours on a rotary shaker at 150 rpm. Then they were centrifuged for 20 minutes at 3500 rpm and the supernatant was discarded. The resins were washed by adding 50 ml of Milli-Q water, shaking for further 30 minutes and centrifugation as before. This process was repeated three

times to remove residuals that may be attached physically on the resins but not retained by chemical binding. The samples were dried by pressurized nitrogen gas (0.4 bar) and a small portion of each dry sample was put on the ATR crystal for ATR-FTIR spectroscopy analysis as illustrated in Figure 2. The samples prepared for the analysis completely covered the ATR crystal and provided a thickness of over 3 μm to eliminate any interference that could be



caused by the compression rod that keeps the samples in place.

Figure 2. Schematic representation of the experimental procedure. Exposing Chelex[®]-100 and Metsorb[™] to Ag and TiO_2 NPs suspensions and their ionic forms for spectral acquisition

2.3 Spectra acquisition and data processing

A PerkinElmer Spectrum 100 FTIR Spectrometer was used for data acquisitions (Figure 2). Each experiment was conducted in triplicate and for each sample, 30 spectra were acquired at 2 cm^{-1} spectral resolution. The IR spectra covered $600\text{--}4000\text{ cm}^{-1}$ range, were divided into three different spectral regions: region one $600\text{--}800\text{ cm}^{-1}$; region two, $800\text{--}2200\text{ cm}^{-1}$; and, region three, $2600\text{--}4000\text{ cm}^{-1}$. To compare the spectral classes, baseline corrections

(rubber band) and vector normalization were used for all of the regions for each treatment. Details of these techniques and available tools to perform these analyses have been described in previous studies.^{33–35}

Following this step, the spectral data were further processed using principal component analysis (PCA) coupled with linear discriminating analysis (LDA), which often referred to as PCA-LDA. PCA and LDA both are statistical procedures and data transformation techniques used in a range of engineering concepts to classify different data and identify patterns. PCA can be described as a linear dimensionality reduction method to project the data into the directions of highest variability (where the data is most spread), while LDA computes the highest possible discrimination between different classes of data which helps us to classify the data accurately.^{36,37}

In this study we used PCA to reduce the number of variables in spectral data (*i.e.*, absorbance intensities at different wavenumbers) to only few factors that can capture >95% variance of the dataset. If the within-class variation is larger than what is found between classes, LDA can be applied to the output from PCA to minimize the within-class variation and maximize between-class variation. This allows us to identify the most important discriminating information and remove interference from the data as described in previous research.^{1,2,33} In other words, this method helps us to identify class differences through the generation of scores and plots. As seen in the next sections, in an LDA scores plot each spectrum represents a point in LDA space and classes tend to form clusters. In these clusters the closeness between points implies spectral similarities while distance signifies class dissimilarities. Also, the plots can be used to identify chemical bonds distinguishing different treatment conditions.

In addition to IR spectroscopy and pattern recognition analysis, we investigated binding of Ag and TiO₂ NPs on Chelex[®]-100 and Metsorb[™] using scanning electron microscope (SEM) to provide further evidence for retention of these NPs on the resins (see ESI for details).

2. Results and Discussion

Figure 3 and 4 show different regions of IR spectra obtained from Chelex[®]-100 and Metsorb[™] after their exposure to silver and titanium dioxide nanoparticles and their ionic forms. As described earlier there are six different spectral classes for each resin, which three of them belong to silver samples; (1) Ag NPs, (2) Ag⁺, (3) mixture of Ag NPs and Ag⁺, and the other three belong to the titanium treatments; (4) TiO₂ NPs, (5) Ti⁴⁺, (6) mixture of TiO₂ NPs and Ti⁴⁺. As seen in these figures clear alterations are observed in different peak absorbance intensities or slight shifts in wavenumbers.

Both of the resins in this study are known for their abilities to bind cations because of their surface functional groups.^{1,8,38} Figure 5 is a schematic representation of potential chemical bonds that may form between the binding agents and Ag⁺ and Ti⁴⁺ cations. Chelex[®]-100 carboxyl and Metsorb[™] surface titanium oxide/hydroxide hydroxyl groups can bind available Ag⁺ and Ti⁴⁺ and irreversibly retain them. Deprotonation of carboxyl groups in Chelex[®]-100 occurs normally at pH ≈ 4.0, thus its overall surface charge in all the experiments with pH ≈ 5.8 is negative.^{2,18} Details of Metsorb[™] chemical structure is not fully disclosed, nevertheless we know that titanium oxides, TiO₂ and Ti(OH)₄ are the main components of this commercial product with TiO₂ dominating. Metsorb[™] point of zero charge is pH ≈ 6.0^{19,39} and has overall neutral to slightly positive surface charge under the current experimental conditions (pH ≈ 5.8). (see ESI for details).

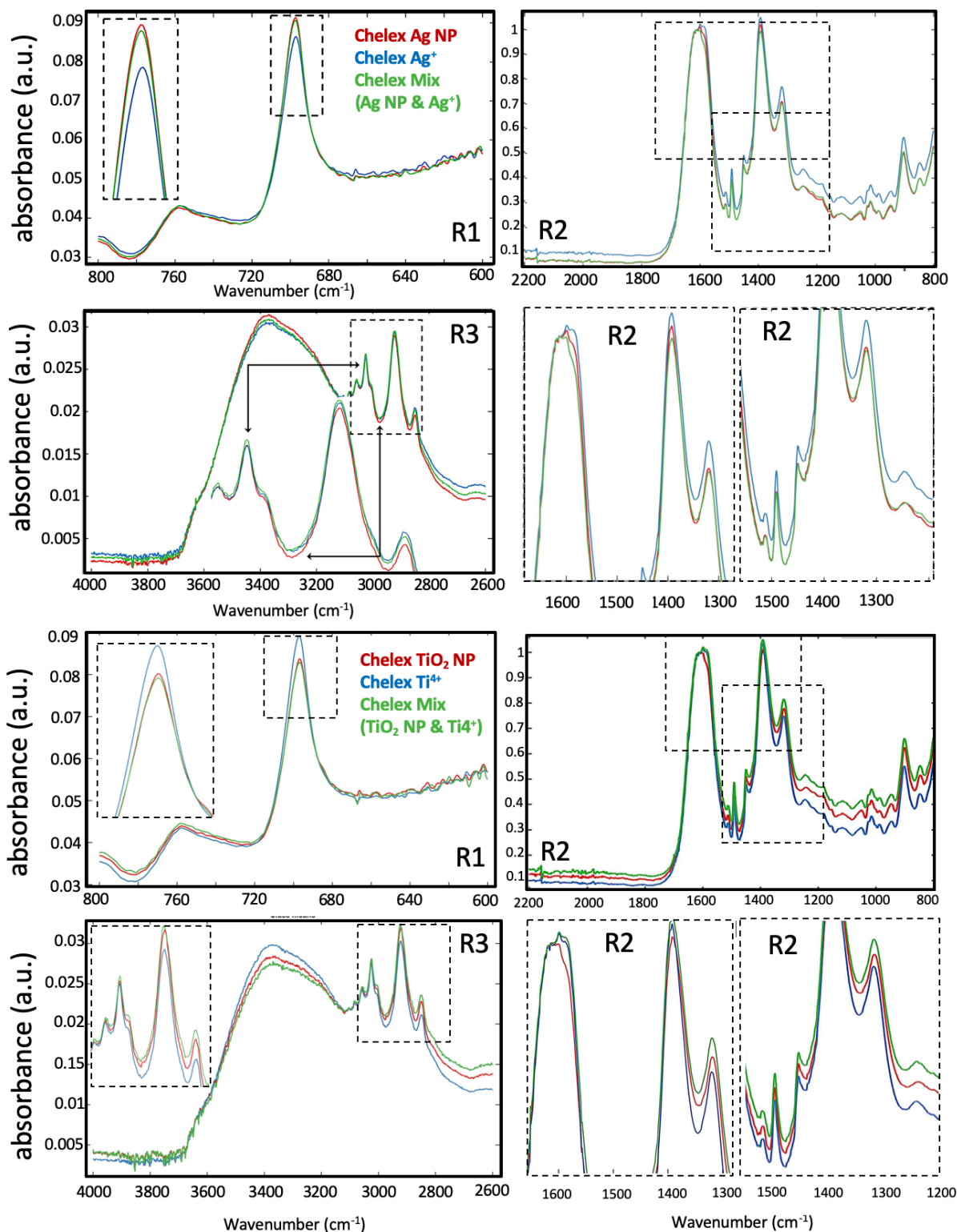


Figure 3. Comparison between derived infrared (IR) spectra for Chelex-100 exposed to the silver and titanium dioxide treatments. The IR spectra (600–4000 cm^{-1}) is divided into three spectral regions: Region 1 (600–800 cm^{-1}), Region 2 (800–2200 cm^{-1}), and region 3 (2600–4000 cm^{-1}) for comparison purpose.

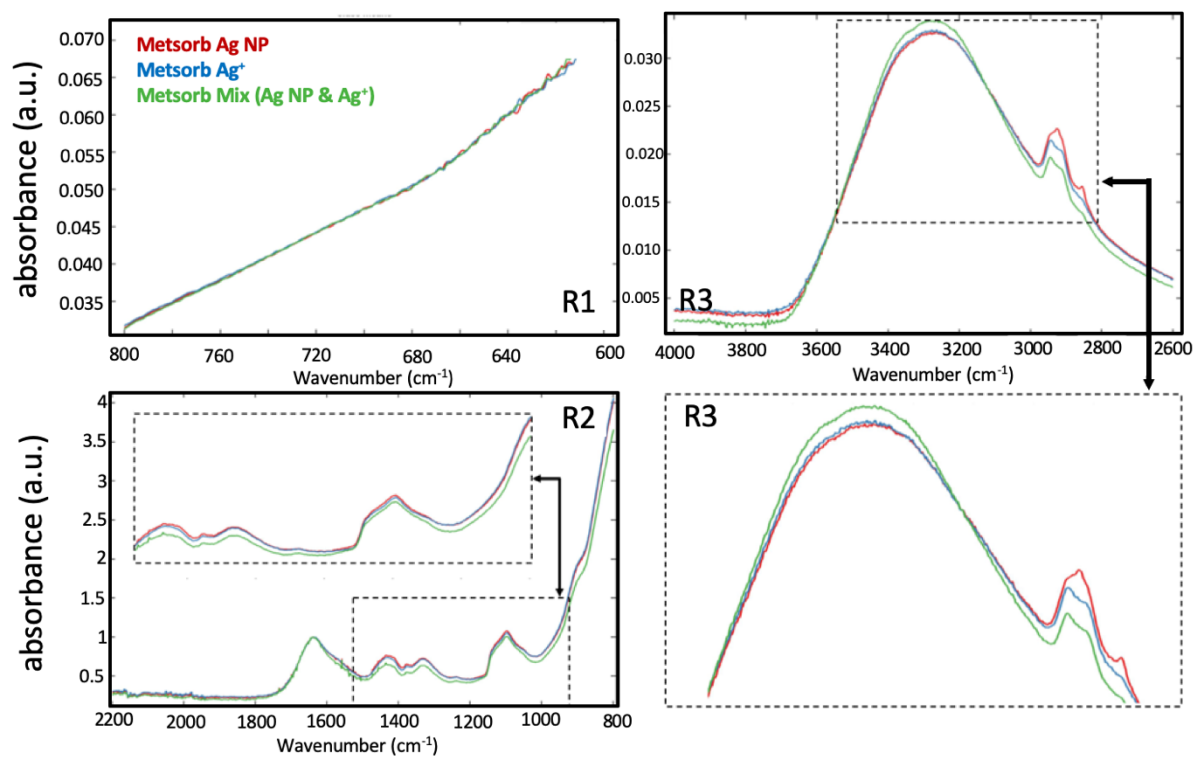


Figure 4. Comparison between derived infrared (IR) spectra for Metsorb exposed to the silver nanoparticle and Ag⁺ treatments. The IR spectra (600–4000cm⁻¹) is divided into three spectral regions: Region 1 (600–800 cm⁻¹), Region 2 (800–2200 cm⁻¹), and region 3 (2600–4000 cm⁻¹) for comparison purpose (see ESI for IR spectroscopy results of Metsorb exposed to titanium dioxide nanoparticles)

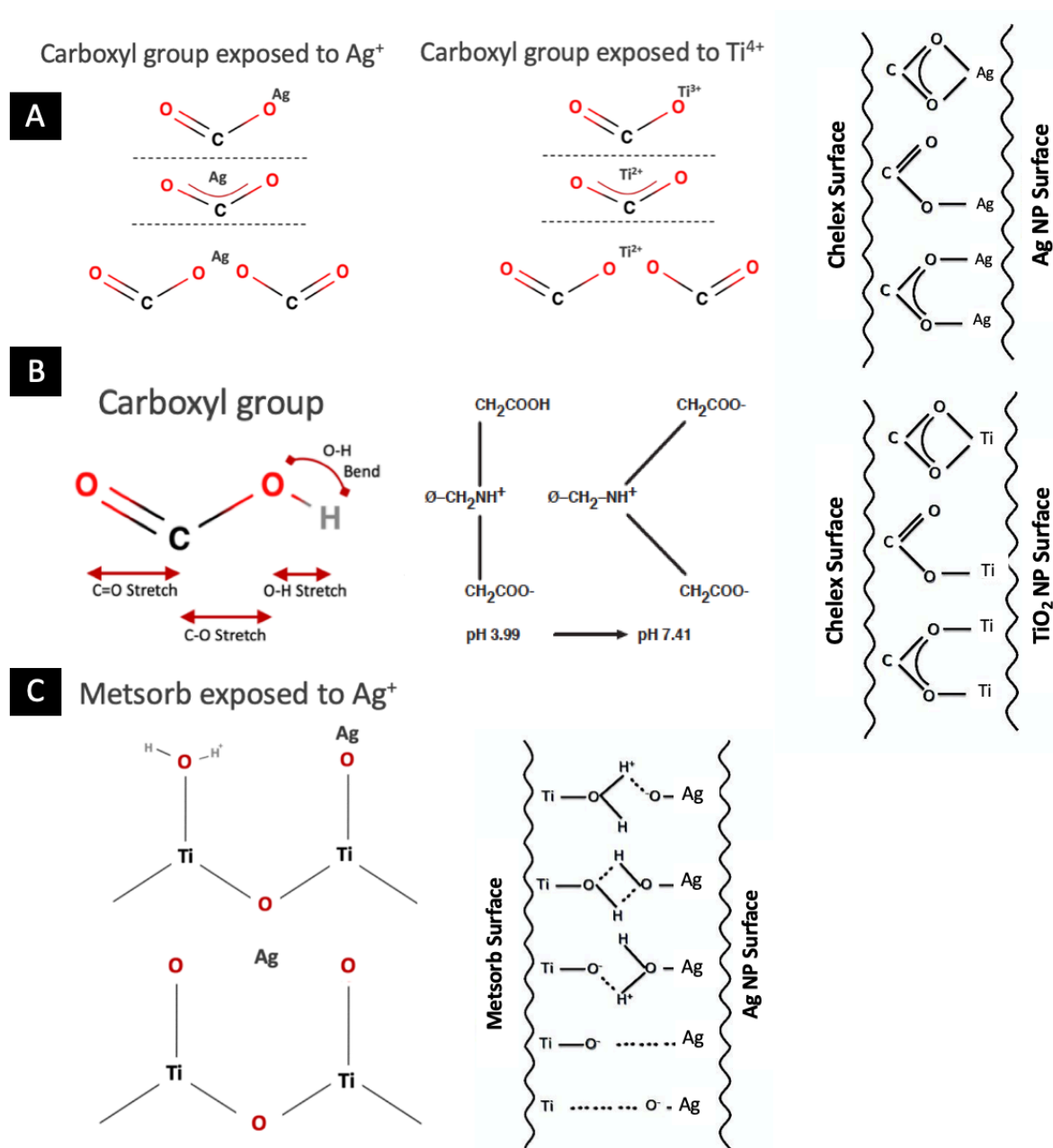


Figure 5. Schematic representation of some of the major chemical bonds that could form between Chelex-100 carboxyl group with Ag^+ and Ti^{4+} (A). Chemical structure of Chelex-100, its deprotonation and carboxyl group potential vibrations (B). some of the major chemical bonds that could form between Metsorb with Ag^+ (C). Also, potential bond formation between the surfaces of Ag, TiO_2 NPs and Chelex-100 or Metsorb have been illustrated on the left side of this Figure.

It's worth noting that at any given pH, both protonated and deprotonated functional groups exist at the same time on the resin surface, but their ratio is affected by the concentration of protons.^{26,40} Deprotonated surface functional groups on Chelex[®]-100, carboxyl groups as seen in Figure 5, could bind Ag⁺ or Ti⁴⁺ directly. Also, two adjacent carboxyl groups are able to chemisorb these cations, while hydroxyl and carbonyl groups together could form complexes with them. Ag NP carries overall negative surface charge in this experiment. Its surface includes oxidized, protonated and deprotonated sites that co-exist at the same time on an Ag NP surface. Chemical bonds could form between protonated surface hydroxyl groups of Ag NPs and deprotonated carboxyl. Other bindings between structural Ag at the surface of Ag NP and carboxyl carbonyl and hydroxyl groups are also possible. The same happens when Chelex[®]-100 is exposed to TiO₂ NPs, however, we know that majority of hydroxyl groups formed on the surface of titanium dioxide nanoparticles are protonated in this study, which could lead to stronger bond formation and retention of this nanoparticle by Chelex[®]-100.

As illustrated in Figure 5, Metsorb[™] surface deprotonated hydroxyl groups could form chemical bonds with Ag⁺. To lesser extent compatible bindings could happen between Metsorb[™] constituent chemicals as well as its surface functional groups with Ag NPs (structural silver and protonated and deprotonated surface hydroxyl groups that form on this nanoparticle surface).^{1,26,27,40}

The afore-mentioned bonding characteristics should be reflected in the vibrational changes of IR spectra of the samples.^{27,41} Figure 3 and 4 represent IR spectra of these chemicals in more details. In spectral region one (600-800 cm⁻¹), Chelex[®]-100 treatments result in a notable alteration at ≈700 cm⁻¹ with clear distinction (peak intensities and slight shift in wavenumbers) between the different classes of spectra, but changes for peak at ≈760 cm⁻¹ seems to be negligible. Interestingly, for Chelex[®]-100 silver and titanium treatments

show different patterns. At $\approx 700\text{ cm}^{-1}$ Ag NPs and the mixture of Ag NPs and Ag^+ have stronger peak (more absorbance) compared to Ag^+ . For the titanium samples, we have an opposite behavior and Chelex[®]-100 exposed to Ti^{4+} has a stronger peak compared to TiO_2 NP or mixture of Ti^{4+} and TiO_2 NPs. The peak at $\approx 760\text{ cm}^{-1}$ is broader, has considerably less strength compared to the one at $\approx 700\text{ cm}^{-1}$ and the observed changes are minor (because of the similarities of the peak intensities). These peaks can be assigned to C-H and N-H vibrations, respectively.^{25,42}

The differences between these peaks at $\approx 700\text{ cm}^{-1}$ could be stemmed from stronger polarity of chemical retention that happens between C-H and Ag NP. Higher number of the same chemical bonds between the resin and Ag NPs, could also contribute to the higher peak intensity. In contrary, it seems that for Chelex[®]-100 titanium treatments, it is Ti^{4+} that creates a stronger dipole moment and therefore stronger peak. For MetsorbTM, the skewed broad peak that is extended to $\approx 800\text{ cm}^{-1}$ can be attributed to metal oxygen bond vibrations that are present in the titanium oxide in MetsorbTM.^{2,43}

In region two of the spectra, Chelex[®]-100 treatments show alterations at $\approx 900\text{ cm}^{-1}$ (C-H out-of-plane bending), $\approx 1330\text{ cm}^{-1}$ (O-C stretching), $\approx 1400\text{ cm}^{-1}$ (C-O-H in plane bending), $\approx 1430\text{ cm}^{-1}$ (O=C-O stretching of carboxylate group), $\approx 1500\text{ cm}^{-1}$ (N-H bending), and $\approx 1620\text{ cm}^{-1}$ (C=O stretching)^{25,26,42}. These changes suggest variations in strength of chemical bonds between oxygen (from C-O, O=C-O and C=O) and; Ag^+ or Ti^{4+} , structural Ag of Ag NPs or Ti of TiO_2 NPs, or the surface hydroxyl groups formed on these nanoparticles. As described earlier MetsorbTM is mainly made of titanium oxide, however, has some impurities including ethanol ($\text{C}_2\text{H}_4\text{O}$)^{2,19}. Bands in the second region of this resin's spectra at $\approx 1100\text{ cm}^{-1}$, $\approx 1350\text{ cm}^{-1}$ and $\approx 1440\text{ cm}^{-1}$ are likely because of C-OH stretch, C-OH and O-H in-plane bend, respectively.^{25,42,43} From these peaks it could be conferred that the surface hydroxyl groups are involved in bond formations with Ag^+ and/or Ag NPs. The peak at $\approx 1650\text{ cm}^{-1}$ can be

attributed to the bending mode of H-O-H, raised from vibration of water or protonation of surface hydroxyl groups.⁴⁴

For Chelex[®]-100 we see a broad O-H stretch peak in the region three, which spans from $\approx 2800\text{ cm}^{-1}$ to $\approx 3600\text{ cm}^{-1}$, N-H stretching vibrations at $\approx 3400\text{ cm}^{-1}$ could also contribute to this peak. Symmetric and asymmetric stretching of C-H and =C-H stretching could be the reason for multiple bands seen at $\approx 2850\text{ cm}^{-1}$, $\approx 2920\text{ cm}^{-1}$ and $\approx 3030\text{ cm}^{-1}$.²⁷ For Metsorb[™] spectra in region three O-H stretching can be identified as a broad peak at $\approx 3100\text{-}3600\text{ cm}^{-1}$ and the other peak, which appears at $\approx 2950\text{ cm}^{-1}$ can be assigned to Ti-OH bending.⁴³ Changes in intensities and shifts in these wavenumbers could be the result of the variations in electrostatic attractions between Ag^+ and structural Ag, surface hydroxyl groups of Ag NPs with functional groups of these vibrational bands.^{1,2} As mentioned earlier, in addition to stronger dipole moments between the bound entities, an increase in peak intensity could be attributed to a rise in the number of functional groups and surface sites associate with the chemical bonds that lead to the observed differences among the samples

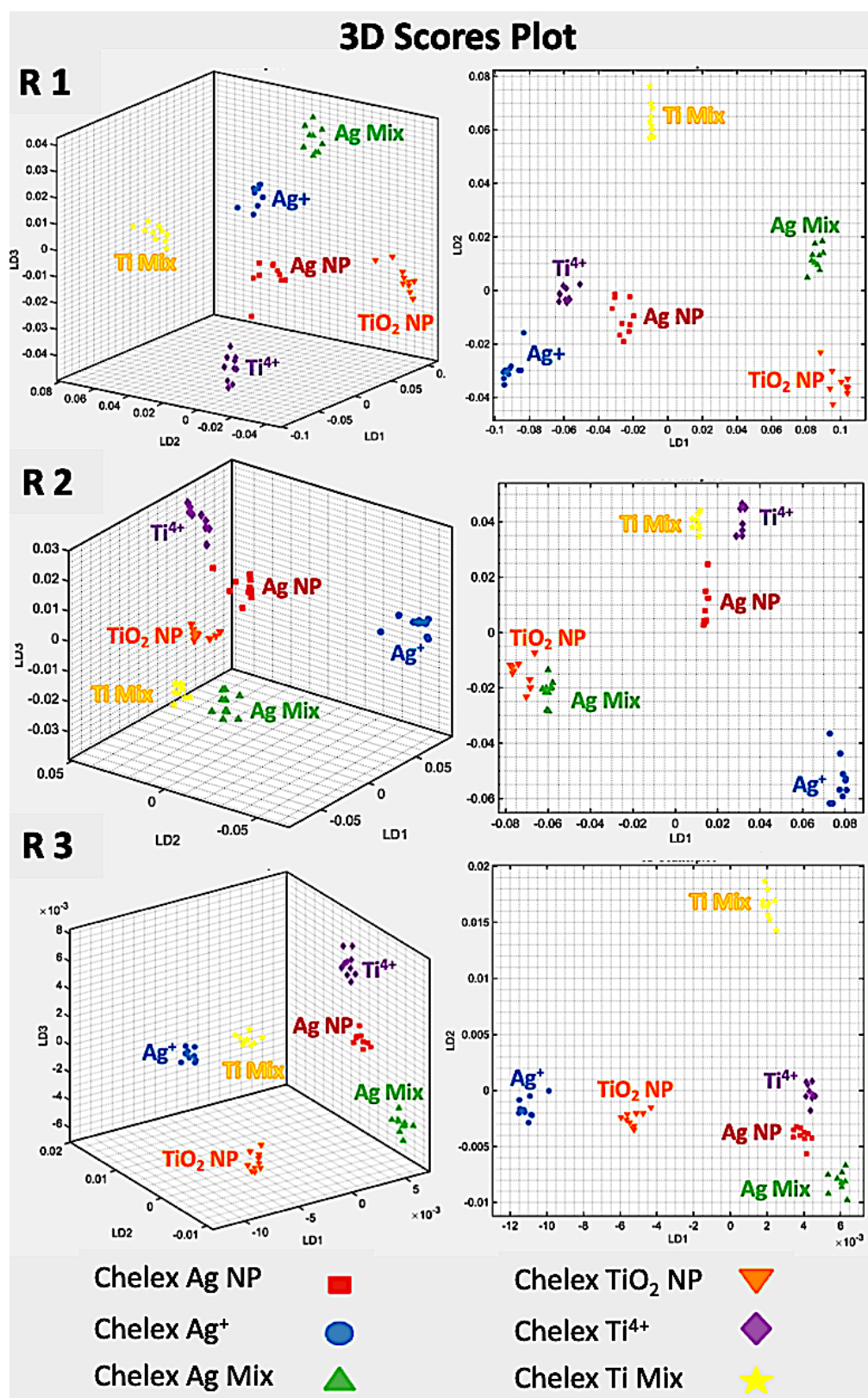
Figure 6 and 7 are 3-D scores plots that exhibit PCA-LDA of absorbance spectra from Chelex[®]-100 and Metsorb[™]. Details of this computational analysis method are available in previous publications.^{2,33-35} As seen multivariate analysis suggests that silver treatments and titanium samples form distinguishable and separate clusters of data in both Chelex[®]-100 and Metsorb[™], which indicate that components of each of these groups have clear differences with each other. In these Figures the 3-D scatter plots separate analyzed (PCA-LDA) IR spectra based on their characteristic differences in their absorbance.^{1,2,33} These analyses demonstrate that for derived spectra for Chelex[®]-100 all of the treatments ; (1) Ag NPs, (2) Ag^+ , (3) mixture of Ag NPs and Ag^+ , (4) TiO_2 NPs, (5) Ti^{4+} , (6) mixture of TiO_2 NPs and Ti^{4+} , are statistically different at the 95% confidence level (for more details see ESI). In other words, these six different spectral classes show statistically different absorbance. For

Metsorb™, as Figure 7 demonstrates, silver samples form three different clusters, which are separated from each other. This segregation indicates that Metsorb™ spectra for these treatments have different characteristics.

In this study the binding mechanisms of the two nanoparticles and their ionic forms to Chelex®-100 and Metsorb™ are affected by the strength and number of chemical bonds formed between them. For Ag^+ and Ti^{4+} the resins are attracting readily available cations, which have similar size to the binding sites on these resins, but for Ag and TiO_2 NPs they are interacting with structural Ag and Ti or functional groups formed on their surfaces including hydroxyls. In addition, Ag NPs carry over all negative surface charge at the pH of the experiment while TiO_2 NPs have overall positive surface pH dependent charge in this experiment (see ESI). Such surface charges influence electrostatic interactions that happen between Chelex®-100 with negative surface charge and Metsorb™ with neutral to slightly positive surface charge at the pH of the experiment ($\text{pH} \approx 5.8$). When Chelex®-100 or Metsorb™ is exposed to Ag or TiO_2 NPs chemisorption occurs between two surfaces, with impacts on the polarity of chemical bonds forming between the two entities as well as the number of functional groups involved in sorption of the NPs, which both influence intensities of the absorbance peaks in the IR spectra. This is compatible to what we observed in the IR spectra of the treatments and deduced through computational analysis and pattern recognition using PCA-LDA technique. It's worth highlighting that this research provides a key finding with respect to diffusive gradients in thin-film (DGT) technique and confirms that Chelex®-100 or Metsorb™ resins, which are of the most common binding materials in DGT devices, are able to form chemical bonds with two of the most extensively used nanomaterials in the world. Considering the well-established DGT technique for measuring time-averaged concentrations of chemicals in the environment, the findings here could pave the road for further development of DGT for measuring Ag and Ti nanoparticles in the

341 environment and helping us to improve our understanding of the fate and the behavior of
342 these materials in nature. In addition to ATR-FTIR spectroscopy and PCA-LDA analysis, we
343 have also used scanning electron microscope (SEM) imaging. The SEM images showed the
344 presence of Ag and TiO₂ nanoparticles on the Chelex[®]-100, however because of the physical
345 appearance and porous structure of Metsorb[™] we couldn't identify these nanoparticles on the
346 surface of this resin. The results can be seen in electronic supplementary information (ESI).

347



348

349 Figure 6. Three-dimensional scores plot visualization of principal component analysis and linear
 350 discriminant analysis (PCA-LDA) of Chelex-100 when exposed to Ag and TiO₂ treatments R1 (600–800 cm⁻¹),
 351 R2 (800–2200 cm⁻¹), and R3 (2600–4000 cm⁻¹), respectively, represent three spectral regions of the
 352 spectra. Scales for X, Y, and Z-axis are arbitrary units. The graphs on the right show the top views of these
 353 scores' plots.

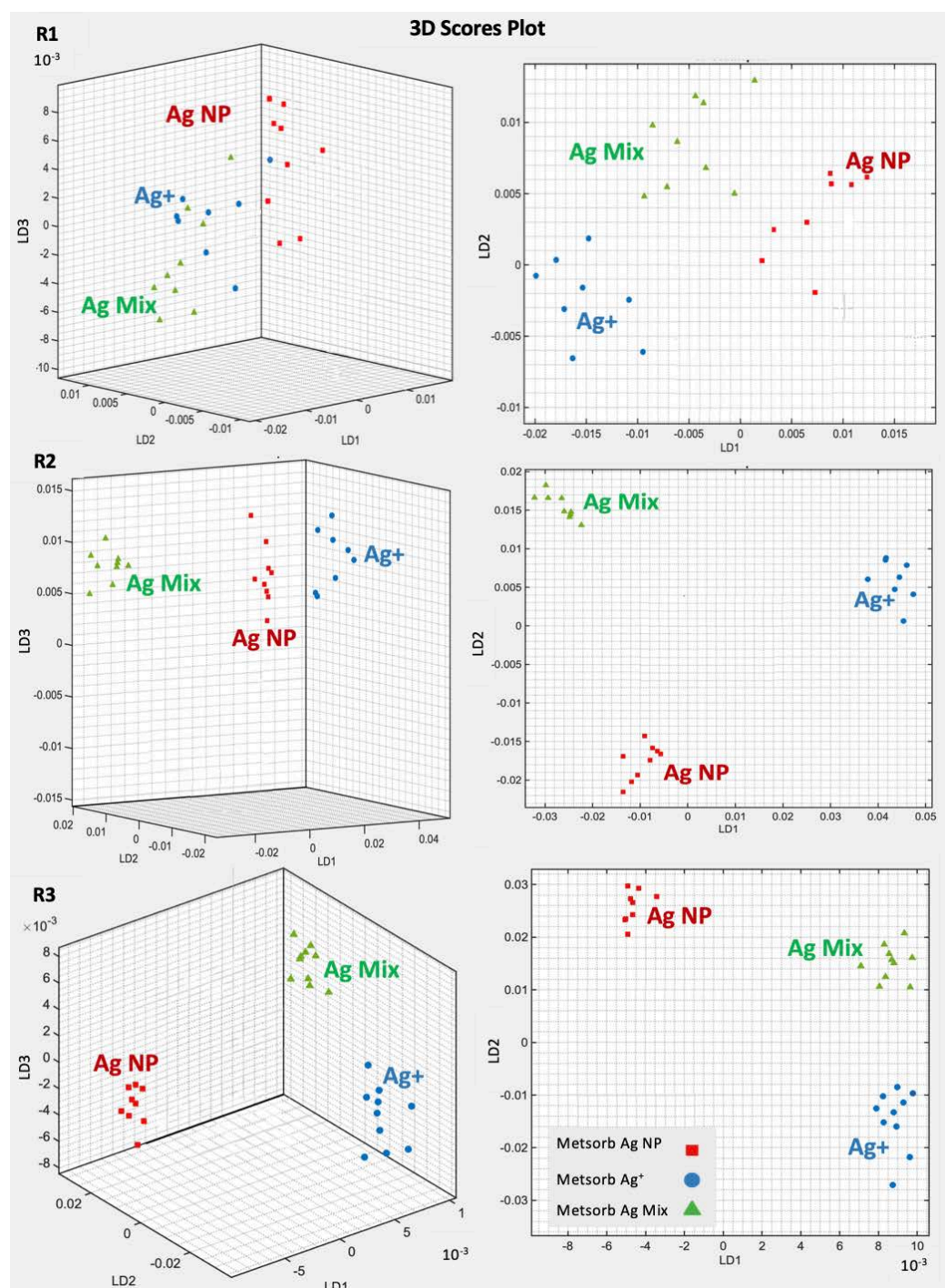


Figure 7. Three-dimensional scores plot visualization of principal component analysis and linear discriminant analysis (PCA-LDA) of Metsorb when exposed to Ag treatments R1 (600–800 cm^{-1}), R2 (800–2200 cm^{-1}), and R3 (2600–4000 cm^{-1}), respectively, represent three spectral regions of the spectra. Scales for X, Y, and Z-axis are arbitrary units. The graphs on the right show the top views of these scores' plots. (see ESI for PCA-LDA scores plot visualization of Metsorb exposed to titanium dioxide nanoparticles)

1. Conclusions

This research shows that Ag and TiO₂ nanoparticles form chemical bonds with Chelex[®]-100 and Metsorb[™], which are two commonly used binding resins in diffusive gradients in thin-film (DGT) method. It is reinforcing our previous findings about DGT potential for measuring engineered nanomaterials in soil and water^{1,2} and is compatible with other studies.⁹⁻¹³ This study also suggests that ATR-FTIR spectroscopy in combination with principal component analysis (PCA) and linear discriminating analysis (LDA), or other pattern recognition methods, could be developed to identify different types of chemicals retained by the binding resins. These give the confidence for using DGT technique measuring nanoparticles in the environment. However, further tests that include investigating diffusional characteristics of model Ag and TiO₂ in the DGT diffusive layers and the performance under a range of environmental conditions are required. of the further development of the DGT technique for measuring engineered nanomaterials in situ in soils and waters would allow us to have a better understanding of their behavior in the environment.

Supporting Information

Electronically supplementary information available: Surface potential of Ag and TiO₂ NPs used in this experiment. Derived infrared (IR) spectra for Metsorb exposed to the titanium dioxide nanoparticle treatments. Three-dimensional scores plot visualization of principal component analysis and linear discriminant analysis (PCA-LDA) of Metsorb exposed to TiO₂ treatments. Two-D visualization of principal component analysis and linear discriminant analysis (PCA-LDA) of Chelex[®]-100 and Metsorb[™] when exposed to silver samples; (1) Ag NPs, (2) Ag⁺, (3) mixture of Ag NPs and the titanium treatments; (4) TiO₂ NPs, (5) Ti⁴⁺, (6)

386 mixture of TiO₂ NPs and Ti⁴⁺. Scanning electron microscope (SEM) imaging of Chelex[®]-100
 387 and Metsorb[™] exposed to Ag and TiO₂ NPs.

388 References

- 389 (1) Pouran, H. M.; Llabjani, V.; Martin, F. L.; Zhang, H. Evaluation of ATR-FTIR
 390 Spectroscopy with Multivariate Analysis to Study the Binding Mechanisms of ZnO
 391 Nanoparticles or Zn to Chelex-100 or Metsorb. *Env. Sci Technol* **2013**, 47 (19),
 392 11115–11121.
- 393 (2) Pouran, H. M.; Martin, F. L.; Zhang, H. Measurement of ZnO nanoparticles using
 394 diffusive gradients in thin films: Binding and diffusional characteristics. *Anal. Chem.*
 395 **2014**, 86 (12), 5906–5913.
- 396 (3) *Diffusive Gradients in Thin-Films for Environmental Measurements*; Davison, W.,
 397 Zhang, H., Eds.; Cambridge University Press: Cambridge, 2016.
- 398 (4) Zhang, H.; Davison, W. In situ speciation measurements. Using diffusive gradients in
 399 thin films (DGT) to determine inorganically and organically complexed metals*. *Pure*
 400 *Appl. Chem* **2001**, 73 (1), 9–15.
- 401 (5) Pouran, H. M. Engineered Nanomaterials in the Environment, their Potential Fate and
 402 Behaviour and Emerging Techniques to Measure Them. In *Handbook of*
 403 *Environmental Materials Management*; Springer International Publishing: Cham,
 404 2018; pp 1–15.
- 405 (6) Baeyens, W.; Gao, Y.; Davison, W.; Galceran, J.; Leermakers, M.; Puy, J.; Superville,
 406 P.-J.; Beguery, L. In situ measurements of micronutrient dynamics in open seawater
 407 show that complex dissociation rates may limit diatom growth. *Sci. Rep.* **2018**, 8 (1),
 408 16125.
- 409 (7) Zhang, H.; Davison, W.; Knight, B.; McGrath, S. In situ measurements of solution
 410 concentrations and fluxes of trace metals in soils using DGT. *Env. Sci Technol* **1998**,
 411 32, 704–710.
- 412 (8) Davison, W.; Zhang, H. Progress in understanding the use of diffusive gradients in thin
 413 films (DGT) - back to basics. *Environ. Chem.* **2012**, 9 (1), 1–13.
- 414 (9) Odzak, N.; Kistler, D.; Behra, R.; Sigg, L. Dissolution of metal and metal oxide
 415 nanoparticles in aqueous media. *Environ. Pollut.* **2014**, 191, 132–138.
- 416 (10) Pham, A. L.-T.; Johnson, C.; Manley, D.; Hsu-Kim, H. Influence of Sulfide
 417 Nanoparticles on Dissolved Mercury and Zinc Quantification by Diffusive Gradient in
 418 Thin-Film Passive Samplers. *Environ. Sci. Technol.* **2015**, 49 (21), 12897–12903.
- 419 (11) Sekine, R.; Brunetti, G.; Donner, E.; Khaksar, M.; Vasilev, K.; Jämting, Å. K.;
 420 Scheckel, K. G.; Kappen, P.; Zhang, H.; Lombi, E. Speciation and Lability of Ag-,
 421 AgCl-, and Ag₂S-Nanoparticles in Soil Determined by X-ray Absorption
 422 Spectroscopy and Diffusive Gradients in Thin Films. *Environ. Sci. Technol.* **2015**, 49
 423 (2), 897–905.
- 424 (12) Liu, S.; Qin, N.; Song, J.; Zhang, Y.; Cai, W.; Zhang, H.; Wang, G.; Zhao, H. A

- nanoparticulate liquid binding phase based DGT device for aquatic arsenic measurement. *Talanta* **2016**, *160*, 225–232.
- (13) Menegário, A. A.; Yabuki, L. N. M.; Luko, K. S.; Williams, P. N.; Blackburn, D. M. Use of diffusive gradient in thin films for in situ measurements: A review on the progress in chemical fractionation, speciation and bioavailability of metals in waters. *Anal. Chim. Acta* **2017**, *983*, 54–66.
- (14) Van Der Veecken, P. L. R.; Pinheiro, J. P.; Van Leeuwen, H. P. Metal speciation by DGT/DET in colloidal complex systems. *Env. Sci Technol* **2008**, *42* (23), 8835–8840.
- (15) Huynh, T.; Zhang, H.; Noller, B. Evaluation and Application of the Diffusive Gradients in Thin Films Technique Using a Mixed-Binding Gel Layer for Measuring Inorganic Arsenic and Metals in Mining Impacted Water and Soil. *Anal. Chem.* **2012**, *84*, 9988–9995.
- (16) Taylor, C.; Matzke, M.; Kroll, A.; Read, D. S.; Svendsen, C.; Crossley, A. Toxic interactions of different silver forms with freshwater green algae and cyanobacteria and their effects on mechanistic endpoints and the production of extracellular polymeric substances. *Environ. Sci. Nano* **2016**, *3* (2), 396–408.
- (17) Philippe, A.; Bundschuh, M.; Klitzke, S.; Rakcheev, D.; Grün, A.; Kumahor, S. K.; Kühn, M.; Manz, W.; Schulz, R. Understanding the fate and biological effects of Ag- and TiO₂-nanoparticles in the environment: The quest for advanced analytics and interdisciplinary concepts. *Sci. Total Environ.* **2015**, *535*, 3–19.
- (18) Bio-RAD. Chelex 100 and Chelex 20 Chelating Ion Exchange Resin Instruction Manual . **2012**, 2012.
- (19) GraverTechnologies. Metsorb MSDS. **2012**.
- (20) Sugimoto, T.; Zhou, X. P. Synthesis of uniform anatase TiO₂ nanoparticles by the gel-sol method - 2. Adsorption of OH⁻ ions to Ti(OH)(4) gel and TiO₂ particles. *J. Colloid Interface Sci.* **2002**, *252*, 347–353.
- (21) Zhu, X. L.; Yuan, C. W.; Bao, Y. C.; Yang, J. H.; Wu, Y. Z. Photocatalytic degradation of pesticide pyridaben on TiO₂ particles. *J. Mol. Catal. a-Chemical* **2005**, *229*, 95–105.
- (22) Panther, J. G.; Teasdale, P. R.; Bennett, W. W.; Welsh, D. T.; Zhao, H. J. Titanium Dioxide-Based DGT Technique for In Situ Measurement of Dissolved Reactive Phosphorus in Fresh and Marine Waters. *Env. Sci Technol* **2010**, *44*, 9419–9424.
- (23) Hutchins, C. M.; Panther, J. G.; Teasdale, P. R.; Wang, F.; Stewart, R. R.; Bennett, W. W.; Zhao, H. Evaluation of a titanium dioxide-based DGT technique for measuring inorganic uranium species in fresh and marine waters. *Talanta* **2012**, *97*, 550–556.
- (24) Turner, G. S. C.; Mills, G. A.; Teasdale, P. R.; Burnett, J. L.; Amos, S.; Fones, G. R. Evaluation of DGT techniques for measuring inorganic uranium species in natural waters: Interferences, deployment time and speciation. *Anal. Chim. Acta* **2012**, *739*, 37–46.
- (25) Pouran, H. M.; Banwart, S. A.; Romero-Gonzalez, M. Characterizing the Cell Surface Properties of Hydrocarbon-Degrading Bacterial Strains, a Case Study.

- 466 (26) Pouran, H. M.; Banwart, S. A. S. A.; Romero-Gonzales, M. Coating a polystyrene
467 well-plate surface with synthetic hematite, goethite and aluminium hydroxide for cell
468 mineral adhesion studies in a controlled environment. *Appl. Geochemistry* **2014**, 42
469 (1986), 60–68.
- 470 (27) Ojeda, J. J.; Romero-Gonzalez, M. E.; Pouran, H. M.; Banwart, S. A. In situ
471 monitoring of the biofilm formation of *Pseudomonas putida* on hematite using flow-
472 cell ATR-FTIR spectroscopy to investigate the formation of inner-sphere bonds
473 between the bacteria and the mineral. *Mineral. Mag.* **2008**, 72 (1), 101–106.
- 474 (28) Chen, C.; Unrine, J. M.; Judy, J. D.; Lewis, R. W.; Guo, J.; McNear, D. H.; Tsyusko,
475 O. V. Toxicogenomic Responses of the Model Legume *Medicago truncatula* to Aged
476 Biosolids Containing a Mixture of Nanomaterials (TiO₂, Ag, and ZnO) from a Pilot
477 Wastewater Treatment Plant. *Environ. Sci. Technol.* **2015**, 49 (14), 8759–8768.
- 478 (29) Lowry, G. V.; Espinasse, B. P.; Badireddy, A. R.; Richardson, C. J.; Reinsch, B. C.;
479 Bryant, L. D.; Bone, A. J.; Deonaraine, A.; Chae, S.; Therezien, M.; et al. Long-Term
480 Transformation and Fate of Manufactured Ag Nanoparticles in a Simulated Large
481 Scale Freshwater Emergent Wetland. *Environ. Sci. Technol.* **2012**, 46 (13), 7027–
482 7036.
- 483 (30) Badawy, A. M. El; Luxton, T. P.; Silva, R. G.; Scheckel, K. G.; Suidan, M. T.;
484 Tolaymat, T. M. Impact of Environmental Conditions (pH, Ionic Strength, and
485 Electrolyte Type) on the Surface Charge and Aggregation of Silver Nanoparticles
486 Suspensions. *Environ. Sci. Technol.* **2010**, 44 (4), 1260–1266.
- 487 (31) AEROSIL® fumed silica [https://products-](https://products-re.evonik.com/www2/uploads/productfinder/AEROXIDE-TiO2-P-25-EN.pdf)
488 [re.evonik.com/www2/uploads/productfinder/AEROXIDE-TiO2-P-25-EN.pdf](https://products-re.evonik.com/www2/uploads/productfinder/AEROXIDE-TiO2-P-25-EN.pdf)
489 (accessed Jan 02, 2019).
- 490 (32) Klitzke, S.; Peters, A. The fate of silver nanoparticles in soil solution — Sorption of
491 solutes and aggregation. *Sci. Total Environ.* **2015**, 535, 54–60.
- 492 (33) Baker, M. J.; Trevisan, J.; Bassan, P.; Bhargava, R.; Butler, H. J.; Dorling, K. M.;
493 Fielden, P. R.; Fogarty, S. W.; Fullwood, N. J.; Heys, K. A.; et al. Using Fourier
494 transform IR spectroscopy to analyze biological materials. *Nat. Protoc.* **2014**, 9 (8),
495 1771–1791.
- 496 (34) Trevisan, J.; Angelov, P. P.; Scott, A. D.; Carmichael, P. L.; Martin, F. L. IRootLab: a
497 free and open-source MATLAB toolbox for vibrational biospectroscopy data analysis.
498 *Bioinformatics* **2013**, 29 (8), 1095–1097.
- 499 (35) Martin, F. L.; Kelly, J. G.; Llabjani, V.; Martin-Hirsch, P. L.; II, P.; Trevisan, J.;
500 Fullwood, N. J.; Walsh, M. J. Distinguishing cell types or populations based on the
501 computational analysis of their infrared spectra. *Nat. Protoc.* **2010**, 5, 1748–1760.
- 502 (36) Martis, R. J.; Acharya, U. R.; Min, L. C. ECG beat classification using PCA, LDA,
503 ICA and Discrete Wavelet Transform. *Biomed. Signal Process. Control* **2013**, 8 (5),
504 437–448.
- 505 (37) Duda, R. O.; Hart, P. E. (Peter E.; Stork, D. G. *Pattern classification*; John Wiley &
506 Sons, 2001.

- 507 (38) Nanosun, M.; 13. ZnO NP Product Application Sheet; Nanosun, Ed.; Micronisers,
508 2012.
- 509 (39) Bennett, W. W.; Teasdale, P. R.; Panther, J. G.; Welsh, D. T.; Jolley, D. F. New
510 Diffusive Gradients in a Thin Film Technique for Measuring Inorganic Arsenic and
511 Selenium(IV) Using a Titanium Dioxide Based Adsorbent. *Anal. Chem.* **2010**, 82,
512 7401–7407.
- 513 (40) Stumm, W.; Morgan, J. J. Aquatic chemistry, chemical equilibria and rates in natural
514 waters. **1996**, 1022.
- 515 (41) Pouran, H. M.; Banwart, S. A.; Romero-Gonzales, M. Preparation of coated
516 polystyrene surfaces with hematite nanoparticles to study cell-mineral adhesion under
517 well-characterized environment. *Geochim. Cosmochim. Acta* **2008**, 72 (2), A758–
518 A758.
- 519 (42) Stuart, B. H. Infrared Spectroscopy Fundamentals And Applications. *Methods* **2004**, 8,
520 224.
- 521 (43) Gao, Y. F.; Masuda, Y.; Seo, W. S.; Ohta, H.; Koumoto, K. TiO₂ nanoparticles
522 prepared using an aqueous peroxotitanate solutions. *Ceram. Int.* **2004**, 30, 1365–1368.
- 523 (44) Kim, W. J.; Veriansyah, B.; Kim, J. D.; Oh, S. G. Formation of titanium hydroxide
524 nanoparticles in supercritical carbon dioxide. *J. Ceram. Process. Res.* **2008**, 9, 88–92.
- 525
- 526